Atmospheric Environment 285 (2022) 119224

Contents lists available at ScienceDirect

Atmospheric Environment

journal homepage: www.elsevier.com/locate/atmosenv

Separately resolving NOx and VOC contributions to ozone formation

Yusheng Zhao [a], Yiting Li [a], Anikender Kumar [b], Qi Ying [c], Francois Vandenberghe [d], Michael J. Kleeman [b],*

[a] *Department of Land, Air, and Water Resource, University of California, Davis, CA, 95616, USA*
[b] *Department of Civil and Environmental Engineering, University of California, Davis, CA, 95616, USA*
[c] *Zachry Department of Civil Engineering, Texas A&M University, College Station, TX, 77843, USA*
[d] *Joint Center for Satellite Data Assimilation, UCAR, Boulder, CO, 80301, USA*

HIGHLIGHTS

- A new method is developed to fully tag NOx and VOC contributions to O_3.
- Tests carried out in LA in 2005, 2010, and 2015 show the method is applicable to any ozone episode.
- Upwind sources and biogenic sources emit most of the VOC that contributes to O_3 formation in LA.
- On-road vehicles and off-road diesel emit most of the NOx that contributes to O_3 formation in LA.
- Given that dominant VOC sources cannot be controlled, NOx controls may be most practical.

ABSTRACT

Ozone (O_3) is widely recognized as a significant air pollutant that affects public health across the globe. O_3 is formed from precursor emissions of oxides of nitrogen (NOx) and volatile organic compounds (VOCs) that react in the atmosphere, making it complex to identify the major source contributions to O_3 concentrations. O_3 source apportionment calculations within chemical transport models (CTMs) provide a specialized approach to resolve source contributions. Traditional O_3 apportionment techniques track source contributions based on the chemical formation regime, but they do not separately distinguish between NOx and VOC source contributions. In this study, a new O_3 source apportionment technique was developed to explicitly resolve the contributions from both NOx and VOC sources in order to provide a more detailed view on O_3 source origins so that policy makers can design more effective emission control strategies. The new technique is flexible and can be configured to identify the original source of precursors that contribute to O_3 formation or the most recent source depending on the choice of the tagging method. The detailed features of the new technique are demonstrated during a peak O_3 event in September 2010 in Los Angeles, while trends in O_3 source contributions over time are evaluated during two additional simulations in July 2005 and August 2015. Quality control checks show that the new source apportionment methodology does not alter predicted total O_3 concentrations, and the detailed source apportionment information can be averaged to yield results that are consistent with traditional O_3 source apportionment calculations. The detailed O_3 source apportionment results during Sept 2010 show that, among NOx sources, on-road gasoline, on-road diesel, off-road diesel, and soil NOx account for over 60% of the ground level O_3 concentrations. Among VOC sources, upwind boundary conditions and biogenic sources account for approximately 90% of the ground-level O_3 formed. The formaldehyde to NO_2 ratio suggests that the chemical regime in the year 2015 was VOC-limited, but given the uncontrollable nature of the VOC emissions, the results suggest that NOx emission controls would have been the preferred emission control strategy to reduce O_3 concentration in Los Angeles at that time, with the understanding that some period of O_3 disbenefits would need to be tolerated until the emissions control program shifts the atmospheric chemistry back into the NOx-limited regime. The NOx source apportionment results for O_3 identify the largest NOx sources that could be reduced in an effort to reach NOx-limited conditions. The chemical regime in the Los Angeles atmosphere is continuously evolving, and so these calculations would need to be repeated under current conditions to determine if we have arrived at this NOx limited regime. Future studies will undertake this analysis.

1. Introduction

Ground-level ozone (O_3) is one of the six criteria pollutants regulated by the United States Environmental Protection Agency (US EPA). O_3 is formed through a complex sequence of photochemical reactions between volatile organic compounds (VOCs) and nitrogen oxides (NOx) in the presence of sunlight (Atkinson, 2000). O_3 harms public health by exacerbating respiratory problems such as coughing, chest tightness,

---

* Corresponding author.
E-mail address: mjkleeman@ucdavis.edu (M.J. Kleeman).

https://doi.org/10.1016/j.atmosenv.2022.119224
Received 3 December 2021; Received in revised form 20 May 2022; Accepted 5 June 2022

and other asthmatic symptoms (Burnett et al., 1997; Gent et al., 2003; Lippmann, 1989). O_3 also damages plants leading to reduced crop yields (Rich, 1964) and harms the built environment by damaging rubber compounds and fading paint (Lee et al., 1996).

O_3 concentrations have decreased significantly over the past 40 years in California due to the adoption of stringent emissions controls, but residual O_3 continues to threaten public health (Faloona et al., 2020). The EPA 2019 design value reports show that there are 74 nonattainment areas violating the 2015 8-Hour O_3 National Ambient Air Quality Standard (NAAQS) across the United States, with 25 of these areas in California.

Understanding source contributions to O_3 formation is a critical first step in the design of efficient O_3 controls in NAAQS nonattainment areas. Both natural and anthropogenic sources can emit O_3 precursors to the atmosphere. Once in the atmosphere, these precursors undergo complex chemical reactions, making it difficult to quantify final source contributions to O_3 formation. One of the specialized approaches developed to handle these complicating factors is species tagging within reactive chemical transport models (CTMs).

Species tagging within CTMs can probe relationships between initial emissions and final concentrations produced by photochemical reaction mechanisms. Species tagging can quantify the contributions from emissions in different geographical regions to concentrations in other geographical regions (Ying and Kleeman, 2006), or emissions in different source categories to the concentrations at receptor locations (Cohan and Napelenok, 2011; Ying et al., 2004; Ying and Kleeman, 2006). Previous studies have performed O_3 source apportionment using the Comprehensive Air Quality Model with extensions (CAMx) with O_3 Source Apportionment Technology (OSAT) (Collet et al., 2014; Li et al., 2012), the EPA's Community Multiscale Air Quality (CMAQ) Integrated Source Apportionment Method (ISAM) (Collet et al., 2018; Kwok et al., 2015), and the Weather Research and Forecasting with Chemistry model (WRF-Chem) (Gao et al., 2016, 2017). The source apportionment methods in these models are very similar. NOx and VOCs are grouped into multiple families and tracked during all the model processes while mass balance is maintained. The production of O_3 is attributed to either VOC or NOx sources depending on the O_3 formation regime. The CAMx-OSAT model and the CMAQ-ISAM model use the ratio of hydrogen peroxide (H_2O_2) production rates to nitric acid (HNO_3) production rates ($P_{H_2O_2}/P_{HNO_3}$) to determine whether O_3 formation is limited by NOx or VOCs (Dunker et al., 2002; Kwok et al., 2015; Tonnesen and Dennis, 2000), while the WRF-Chem model uses the ratio of HCHO/NOy (Sillman, 1995). Once the O_3 formation regime is determined, the contributions of O_3 are attributed to different source groups based on the ratio of the limited precursor in the source group to the total limited precursors in all source groups.

Attributing O_3 formation to the sources of the limiting precursor makes the source apportionment results easier to interpret, but ignoring the separate roles that NOx and VOC sources play in O_3 formation can miss important features. The dominant sources of NOx in the VOC-limited regime or the dominant sources of VOC in the NOx-limited regime are relevant and important to understand when designing an efficient emissions control program to reduce O_3 concentrations. For example, conventional wisdom states that reducing VOC emissions is the most effective way to control O_3 formation when NOx is abundant. Reducing NOx in this regime may cause O_3 concentrations to increase in the short term. However, this simplified view ignores cases under which VOC cannot be reduced because further controls are too expensive or impractical. Understanding the contributions from both NOx and VOC sources in the context of the O_3 formation regime is therefore necessary for the design of effective emission control programs.

Here we propose a new O_3 source apportionment technique within the framework of a regional CTM to address shortcomings in the traditional O_3 source apportionment approaches by fully apportioning NOx and VOC contributions to O_3 concentrations.

2. Methodology

2.1. Model configuration

The University of California Davis/California Institute of Technology (UCD/CIT) air quality model was used to predict the O_3 source apportionment results. The UCD/CIT air quality model is a reactive chemical transport model (CTM) that predicts the evolution of gas- and particle-phase pollutants with emissions, transport, deposition, chemical reaction, and phase change (Kleeman and Cass, 2001; Yu et al., 2019). The model solves the core equation

$$\frac{\partial C_i}{\partial t} + \nabla \cdot uC_i = \nabla K \nabla C_i + E_i - S_i + R_i^{gas}(C) + R_i^{particle}(C) + R_i^{phase}(C)$$

where C_i is the concentration of gas- or particle-phase species i at a particular location as a function of time t, u is the wind vector, K is the turbulent eddy diffusivity tensor (assumed to be diagonal), E_i is the emissions rate, S_i is the loss rate, R_i^{gas} is the change in concentration due to gas-phase reactions, $R_i^{particle}$ is the change in concentration due to particle-phase reactions, and R_i^{phase} is the change in concentration due to phase change.

The UCD/CIT model can be configured to use any gas-phase chemical mechanism. Gas-phase chemistry in the current study is described using two versions of the SAPRC11 chemical mechanism (Carter and Heo, 2013). The first version of SAPRC11 was configured to track NOx source contributions to O_3 formation, while the second version was configured to track VOC source contributions to O_3 formation. Both versions of the mechanism enforce mass balance.

O_3 source apportionment results were calculated for Los Angeles from Sep 21 to Sep 27, 2010, corresponding to the highest regional O_3 concentrations in Southern California in this year (Venecek et al., 2019). Two domains were used in the simulation: one parent domain with 24-km resolution covers all of California, and one subdomain with 4-km resolution covers southern California (Fig. S1). Meteorology inputs were generated by the Weather Research and Forecasting (WRF) model (WRFv3.4). Anthropogenic emissions were generated based on the California Air Resource Board (CARB) 2010 Emission Inventory processed using the Sparse Matrix Operator Kernel Emissions (SMOKEv3.7). Biogenic emissions were generated using the Model of Emissions of Gases and Aerosols from Nature (MEGANv2.1). Initial and boundary conditions were generated from the global concentration field predicted by the Model for Ozone and Related chemical Tracers (MOZART).

2.2. NOx source apportionment

The NOx source apportionment (NOx SA) method follows the tagging approach previously used to track source contributions to particulate nitrate formation (Kleeman et al., 2005). Nitrogen atoms contained in NOy species NO, NO_2, NO_3, N_2O_5, HNO_3, HNO_4, PAN, etc., are automatically tagged with the source suffix _N using a modified version of the "prep" mechanism compiler distributed as part of the SAPRC software suite. The current formulation expands the method to include O^3P, O^1D, and O_3 using nitrogen source tags that are passed from NOx species. The automated process enforces tag balance so that the total number of tags is identical for reactants and products. For example, the SAPRC11 reaction

NO2 + NO3 = N2O5

is automatically expanded to

NO2_N1 + NO3_N2 = N2O5_N1_N2

Two special cases do not follow the tag balance rules and must be handled separately. The first special case passes the nitrogen source tag information from the reactant NO_2 or NO_3 species with a single tag to the product NO or NO$_2$ species and to the product O^{3}P species. Reactions following this pattern are listed in Table 1.

The second special case passes the source tag information from the reactant NOx species and discards the source tag information from the reactant O$_3$ or O^{3}P species. The reaction templates for this case are listed in Table 2.

Although the two special cases purposefully do not enforce source tag balance, they still follow the mass balance, and all reactions conserve the total concentrations of reactive nitrogen species and odd oxygen species. A total of nine source tags representing different emission source groups are used in the current NOx source apportionment exercise, leading to the expanded reaction count listed in the final columns of Tables 1 and 2 The combined automatic tagging procedures and the special case tagging procedures summarized in Tables 1 and 2 produce 2439 tagged chemical reactions with nine source tags in addition to the base SAPRC11 mechanism.

2.3. VOC source apportionment

The VOC source apportionment (VOC SA) tagging approach is similar to the NOx source apportionment approach but tags are used to track sources of odd oxygen instead of nitrogen. VOCs emitted from different source groups are tagged with the suffix _X. Each tag is then passed to the peroxy radicals and other compounds containing odd oxygen produced in the chemical reactions. The complexity of the VOC reactions produces multiple special cases that cannot balance the oxygen tag between reactants and products. Reaction templates are used to specify the tagging pattern in these cases, as described below.

The first special case involves reactions that have one single-tag reactant but multiple tagged products. The single reactant tag is passed to all the specified tagged products in this case. For example, the following reaction in SAPRC11

RO2XC + MEO2 = #.5 HO2 + #.75 HCHO + #.25 MEOH

is tagged with the template

RO2XC + MEO2_X1 = #.5 HO2_X1 + #.75 HCHO_X1 + #.25 MEOH_X1

For reactants involving two VOCs, source tags are evenly distributed to the products. For example, the following reaction in SAPRC11

MECO3 + MEO2 = #.1 CCOOH + #.1 HCHO + #.1 O2 + &

#.9 HCHO + #.9 HO2 + #.9 MEO2 + #.9 CO2

is tagged with the template

MECO3[_X1] + MEO2[_X2] = #.05 CCOOH[_X1] + &

#.05 CCOOH[_X2] + #.5 HCHO[_X1] + #.1 O2 + &

#.5 HCHO[_X2] + #.45 HO2[_X1] + #.45 HO2[_X2] + &

#.45 MEO2[_X1] + #.45 MEO2[_X2] + #.9 CO2

where _X1 represents source tag1 and X2 represents source tag2.

Table 1

Reactions of the first special case to track NOx-source contributions to O$_3$ formation. Only the first typed reaction in each sequence is shown to be concise. The total number of reactions matching each format is shown in the far right column when tracking contributions from nine sources plus initial/boundary conditions.

Reaction Label	SAPRC11 Rate Constant	Modified Reaction	Total Prep Reactions
1-N	PF=NO2-06	NO2_N1 + HV = NO_N1 + O3P_N1	9
17-N	PF=NO3NO2-6	NO3_N1 + HV = NO2_N1 + O3P_N1	9

Table 2

Reaction templates for the second special case to track NOx-source contributions to O$_3$ formation. The source tags _N[1–9] in the reactants are matched to the source tags in the product list. The total number of additional reactions matching each format is shown in the far right column when tracking contributions from nine sources plus initial/boundary conditions.

Reaction Label	SAPRC11 Rate Constant	Modified Reaction	Total Prep Reactions
4O3+N	FALLOFF 9.00e-32 0.000–1.50 3.00e-11 0.000 0.00 0.60 1.00	O3P[_N1] + NO[_N2] = NO2[_N2]	99
5O3+N	5.50e-12 -0.374 0.00	O3P[_N1] + NO2[_N2] = NO[_N2] + O2	99
6O3+N	FALLOFF 2.50e-31 0.000–1.80 2.20e-11 0.000–0.70 0.60 1.00	O3P[_N1] + NO2[_N2] = NO3[_N2]	99
7O3+N	3.00e-12 2.981 0.00	O3[_N1] + NO[_N2] = NO2[_N2] + O2	99
8O3+N	1.40e-13 4.908 0.00	O3[_N1] + NO2[_N2] = O2 + NO3[_N2]	99

In cases where specific products can be traced to the specific reactants, the source tag of that products is the same as the specific reactants. For example, the following reaction in SAPRC11

BZCO3 + RO2C = RO2C + BZO + CO2

is tagged with the template

BZCO3[_X1] + RO2C[_X2] = #.5 RO2C[_X1] + #.5 RO2C[_X2] + BZO [_X1] + CO2

where RO2C can be traced to both reactants, and BZO can be traced to BZCO3 based on the BZCO3 chemistry in SAPRC11 mechanism.

For parent VOCs and peroxy radicals reacting with tagged O$_3$ or O^{3}P, the source tag in O$_3$ and O^{3}P is only passed to half of HO$_2$ and xHO$_2$ products. The rest of the products are tagged with the identity of the parent VOC or peroxy radical. For example, the following reaction in SAPRC11

ISOPRENE + O3 = #.266 OH + #.066 HO2 + &

#.192 RO2C + #.008 RO2XC + #.008 zRNO3 + #.275 CO + &

#.122 CO2 + #.4 HCHO + #.1 PROD2 + #.39 MACR + &

#.16 MVK + #.15 IPRD + #.204 HCOOH + &

#.192 xMACO3 + #.192 xHCHO + #.2 yR6OOH + &

#-1.000 XC + #0.401 XC

is tagged with the template

ISOPRENE[_X1] + O3[_X2] = #.266 OH + #.033 HO2[_X1] + &

#.033 HO2[_X2] + #.192 RO2C[_X1] + #.008 RO2XC + &

#.008 zRNO3[_X1] + #.275 CO + &

#.122 CO2 + #.4 HCHO[_X1] + #.1 PROD2[_X1] + #.39 MACR[_X1] + &

#.16 MVK[_X1] + #.15 IPRD[_X1] + #.204 HCOOH[_X1] + &

#.192 xMACO3[_X1] + #.192 xHCHO[_X1] + #.2 yR6OOH[_X1] + &

#-1.000 XC + #0.401 XC

When odd oxygen is passed to reactive nitrogen compounds, the original VOC source tags are also preserved since they will eventually be passed from reactive nitrogen compounds back to O_3. The reactive nitrogen species that contain odd oxygen are NO_2, NO_3, N_2O_5, PAN-species, HNO_4, RNO_3, and $xRNO_3$. For reactions that have both tagged parent VOC and tagged reactive nitrogen compounds as reactants, the source tags in the nitrogen compounds are only passed to reactive nitrogen compound in the products. The rest of the products are tagged with the source identity of the VOC reactants. For example, the following reaction in SAPRC11

MEO2 + NO3 = HCHO + HO2 + NO2

is tagged with the template

MEO2[_X1] + NO3[_X2_X3] = HCHO[_X1] + HO2[_X1] + &

#.5 NO2[_X2] + #.5 NO2[_X3]

For photolysis reactions involving PAN species with two source tags, the two source tags are evenly distributed to the products. For example, the following reaction in SAPRC11

PAN + HV = #.6 MECO3 + #.6 NO2 + #.4 MEO2 + #.4 CO2 + #.4 NO3

is tagged with the template

PAN[_X1_X2] + HV = #.3 MECO3[_X1] + #.3 MECO3[_X2] + &

#.3 NO2[_X1] + #.3 NO2[_X2] + &

#.2 MEO2[_X1] + #.2 MEO2[_X2] + &

#.4 CO2 + #.4 NO3[_X1_X2]

The number of variables and reactions within the SAPRC11 mechanism grows non-linearly with the number of tracked VOC sources. A total of six VOC source tags were tracked in the current study with the upper bound constrained by the limits of the FORTRAN compiler on the host computer system. The combined SAPRC11 mechanism generated using automatic tag balancing along with the reaction templates described above contained 18132 tagged reactions in addition to the base SAPRC11 mechanism.

2.4. *Model refinements to support source apportionment calculations*

2.4.1. *Advection equation solver*

Source apportionment calculations embedded into Chemical Transport Models (CTMs) should not change the predicted total concentrations of the tagged species (Dunker et al., 2002). Achieving this consistent behavior can be challenging for some model processes such as advection. Many CTMs decompose the 3D advection problem into a series of 1D advection problems described by the equation

$$\frac{\partial C}{\partial t}+\frac{v\partial C}{\partial x}=0$$

where C is the concentration, t is time, and v is the velocity in the direction of interest. Numerical solutions to the advection equation produce numerical noise that degrades the accuracy of the predicted pollutant concentration fields around sharp concentration gradients. Chock (Chock, 1985, 1991; Chock and Dunker, 1983) investigated multiple algorithms for solving the advection equation and found that the Forester (1977) smoothing scheme can be used to dampen computational noise around sharp wave fronts. The method approximates a diffusive process selectively applied in regions of oscillating concentrations using the equation

$$C_i^{k+1}=C_i^k+(\mu/2)\left(\Delta C_{i+1/2}(\varphi_i+\varphi_{i+1})-\Delta C_{i-1/2}(\varphi_i+\varphi_{i-1})\right)^k$$

where i is the grid cell location and k is the smoothing application count, $k=1$ for atmospheric modeling; μ is diffusion coefficient (typically <0.5); $\Delta C_{i-1/2}\equiv C_i-C_{i-1}$; φ is the grid function variable, $\varphi=1$ for grid locations around oscillating concentrations where smoothing is required and $\varphi=0$ for the other grid locations. Separating parent NOx or VOC species into source-oriented groups naturally creates sub-group fields with sharp spatial gradients. The spatial pattern of numerical noise that develops around these fields can change according to the source-apportionment configuration. This leads to slightly different results from advection calculations carried out using different source apportionment configurations. This undesirable behavior was corrected by modifying the Forester smoothing algorithm so that the spatial smoothing pattern (φ_i values) for all source-oriented concentrations within the same parent species were based on the spatial patterns of the total parent species concentrations (summed across all source-oriented groups). The consistent smoothing pattern (φ_i values) applied to all source-oriented species within the same parent family regardless of the source-apportionment configuration largely produces consistent results across the advection calculations.

2.4.2. *Simplified tagging mechanism*

To enable our source apportionment technique to track nine emission source sectors simultaneously, we simplified both NOx SA and VOC SA by modifying multi-tagged species to single-tagged species. The reaction templates are also modified to be compatible with the simplified method. For example, the tagged template in NOx SA

NO2_N1 + NO3_N2 = N2O5_N1_N2

is modified to

NO2_N1 + NO3_N2 = #.5 N2O5_N1 + #.5 N2O5_N2

The tagged template in VOC SA

O3_X1 + NO2_X2 = O2 + NO3_X1_X2

is modified to

O3_X1 + NO2_X2 = O2 + #.5 NO3_X1 + #.5 NO3_X2

The simplified tagging mechanism has reduced the number of tagged chemical reactions from 2836 to 2566 in NOx SA and 18132 to 11782 in VOC SA in addition to the base SAPRC11 mechanism, respectively.

2.5. *Model comparison with CMAQ-ISAM*

O_3 source apportionment results from the UCD/CIT model were also compared to the results generated by the CMAQ-ISAM model developed by the United States EPA. The model configuration during this comparison test was similar to the configuration described in section 2.1 with the exception that a single domain with 12 km spatial resolution covering Southern California was used to expedite the calculations. The anthropogenic emissions were generated from the SMOKEv3.7 using the 2011 National Emission Inventory (NEI). CMAQ-ISAM used the saprc07tic_ae7i_aq chemical mechanism while UCD/CIT used SAPRC11 (Carter and Heo, 2013). For aerosol-phase chemical mechanism, CMAQ-ISAM used AERO7 while UCD/CIT used ISSOROPIA for inorganics and n-product model with adjusted coefficients for SOA. A summary comparing the model details is provided in Table S1.

3. Results

3.1. *Model improvements*

3.1.1. *Advection equation solver*

Simulations over California were performed using different VOC source apportionment configurations to test the effects of the updated Forester smoothing algorithm during an 8-day period in Aug 2009 (Aug 21–28). Fig. 1 shows four concentration difference plots for NO_2 at hour 12 on the final simulation day. Each panel of Fig. 1 shows the difference

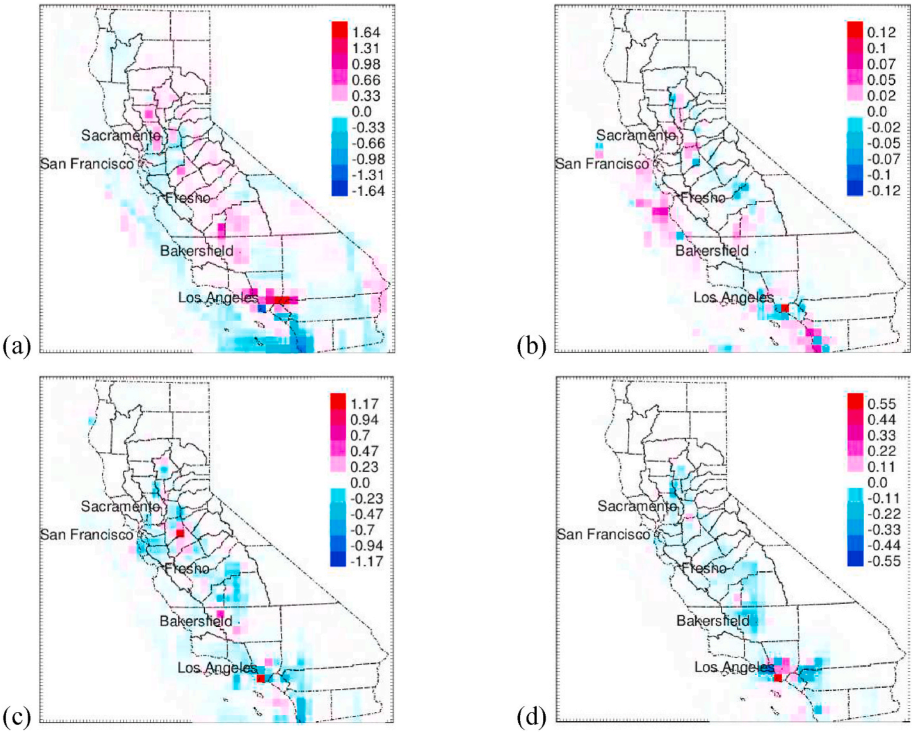

Fig. 1. NO_2 difference plots at hour 12 on August 28, 2009 for test cases with (a) chemical reactions off and no uniform smoothing pattern; (b) chemical reaction off and uniform smoothing pattern applied; (c) chemical reactions on and no uniform smoothing pattern; (d) chemical reaction on and uniform smoothing pattern applied. All units ppb.

in NO_2 concentrations between a simulation with source apportionment (SA) and a simulation without source apportionment (NonSA). The top row of Fig. 1 is configured with chemical reactions disabled while the bottom row is configured with chemical reactions enabled. The left column of Fig. 1 is configured using the original Forester smoothing algorithm while the right column is configured using the updated algorithm. The results displayed in the top row of Fig. 1 indicate that adoption of the updated Forester smoothing algorithm reduces the maximum value of the computational noise in the NO_2 concentrations from 1.64 ppb to 0.12 ppb in the absence of chemical reactions. NonSA NOx concentrations range from 0.09 ppb to 5.51 ppb with a mean value of 0.95 ppb in these simulations. The bottom row of Fig. 1 shows that the adoption of the new Forester smoothing algorithm reduces the maximum value of the computational noise in the NO_2 concentrations from 1.17 ppb to 0.55 ppb when chemical reactions are enabled. NonSA NOx concentrations range between 0.08 ppb and 29.96 ppb with a mean value of 1.60 ppb in these simulations.

3.1.2. *Simplified tagging mechanism*

Fig. 2 illustrates the difference in total O_3 concentrations predicted at hour 12 of each day September 21–27, 2010 using source apportionment with simplified tagging mechanism (Simp) and without simplified mechanism (NoSimp). Concentration differences are shown as box and whisker plots across all grid cells in the model domain as a function of simulation date. Four source apportionment configurations are tested: (NOx SA or VOC SA) × (NoSimp or Simp). Detailed statistical comparisons are presented in Table S2 and Table S3, with mean bias varying from -0.0731 to 0.1654 ppb and mean error varying from 0.0178 to 0.1660 ppb. All the source-apportionment configurations have similar accuracy compared to results generated without source apportionment. These findings suggest that the simplified tagging mechanisms can be adopted to achieve improved computational efficiency with little loss of overall accuracy.

Fig. S2 and Fig. S3 show the field plots comparing O_3 contributions from different sources for hour 12 of the last simulation day. For both NOx SA and VOC SA, the source apportionment results have negligible change, indicating that the simplified method changes neither the total O_3 concentrations nor the source contributions to O_3. For VOC SA, we separate gasoline, diesel, and woodsmoke and food cooking emission sectors into six emission sectors, giving more details of source apportionment information.

3.2. *Evaluation of ozone source apportionment technique in UCD/CIT model*

3.2.1. *Model results without SA technique*

Table 3 part (a) presents the model performance statistics for CMAQ and UCD model predictions compared to measured concentrations. The locations of the four measurement sites used for the analysis are shown in Fig. S1. When comparing the daily maximum 8-h average O_3 at the four sites, NMB values are 0.1184 for CMAQ and 0.0819 for UCD/CIT, and NME values are 0.1954 for CMAQ and 0.2020 for UCD/CIT, which meet the performance criteria typically used for CTM calculations (Emery et al., 2017). Correlation coefficients (r) are 0.7633 for CMAQ and 0.8567 for UCD/CIT, which meets the performance goals. Further analysis of performance statistics using 1-h O_3 is shown in Table S4. In general, both CMAQ and the UCD/CIT model predicted O_3 concentrations with reasonable accuracy. Fig. S4 illustrates the time series plots of O_3 predictions and measurements at individual monitoring sites.

3.2.2. *Model results with SA technique*

Fig. 3 illustrates the source apportionment results of CMAQ-ISAM-O3 and UCD/CIT SA at four monitoring sites. Ozone source contributions predicted using the same model are similar at all locations. Boundary conditions and initial conditions (BCIC) make the largest contributions to O_3 formation at all sites. The 30–50 ppb of background O_3 advected into California accounts for the majority of the BCIC contribution in both the NOx and VOC source apportionment calculations. CMAQ-ISAM-O3 results also identify BCIC as the single largest contributor to O_3 concentrations during the study period. For CMAQ-ISAM-O3 source

Table 3

Model performance statistics for daily maximum 8-h average O_3 at different sites in (a) CMAQ and UCD/CIT evaluation runs in September 2010; (b) UCD/CIT source apportionment runs in September 2010; (c) UCD/CIT source apportionment runs in July 2005; (d) UCD/CIT source apportionment runs in August 2015.

		NMB	NME	r
(a) 12 KM runs using NEI2011 in September 2010	CMAQ	0.1184	0.1954	0.7633
	UCD/CIT	0.0819	0.2020	0.8567
(b) 4 KM UCD/CIT SA runs using CARB emission inventory in September 2010	NOx SA	0.0430	0.1097	0.9310
	VOC SA	0.0372	0.1086	0.9307
(c) 4 KM UCD/CIT SA runs in July 2005	NOx SA	−0.1211	0.1489	0.9058
	VOC SA	−0.1136	0.1454	0.9059
(d) 4 KM UCD/CIT SA runs in August 2015	NOx SA	0.1871	0.2137	0.4882
	VOC SA	0.1828	0.2102	0.4901

Note: For model performance of daily maximum 8-h average O_3, "Goals" are NMB<±5%, NME<15%, $r > 0.75$, which should be viewed as the best a model can be expected to achieve. "Criteria" are NMB<±15%, NME<25%, $r > 0.50$, which should be viewed as what a majority of models have achieved (Emery et al., 2017).

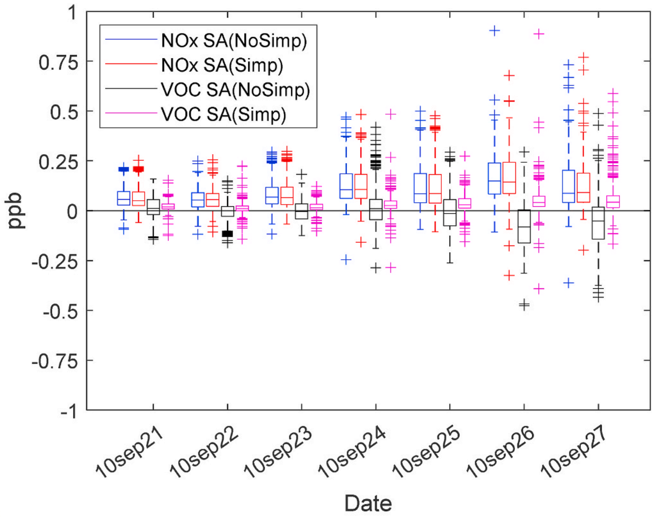

Fig. 2. Total O_3 differences between results with SA and results without SA across the whole domain at hour 12 for the indicated days in September 2010.

apportionment results, off-road gasoline, off-road diesel, natural gas, biogenics, and other emission sectors make notable contributions to O_3 formation. On-road gasoline, on-road diesel, and wood smoke emission sectors make smaller contributions to the O_3 formation, while the food cooking sector makes negligible contributions to the O_3 formation.

For UCD/CIT-NOx source apportionment results, NOx emissions from the off-road diesel sector make the second largest contribution to the O_3 formation. NOx emissions from off-road gasoline, natural gas, and other emission sectors also contribute to O_3 formation. NOx emissions from on-road gasoline, on-road diesel, wood smoke, and food cooking make negligible contributions to the O_3 formation.

For UCD/CIT-VOC source apportionment results, VOC emissions from the biogenic sector contribute significantly to the O_3 formation. VOCs in off-road gasoline and other emissions sector make minor contributions to the O_3 formation. On-road gasoline, on-road diesel, off-road diesel, wood smoke, food cooking, and natural gas sources make negligible contributions to the O_3 formation.

CMAQ-ISAM-O3 source apportionment calculations simultaneously track both NOx and VOC contributions to O_3 formation, while the UCD/CIT model separately tracks NOx and VOC contributions. The rank order of sources that contribute to O_3 formation is identical in the CMAQ-ISAM-O3 results and the combined results from the UCD/CIT calculations (Fig. S10). A further consistency check between the two models was carried out by configuring the CMAQ-ISAM model for separate NOx and VOC tagging so that results could be directly compared to the UCD/CIT model for intermediate species, including NO, NO2, and HCHO. The comparison illustrated in Figures S5 through S7 show that the CMAQ-ISAM predictions are similar to the UCD/CIT model predictions, confirming that the model calculations are consistent. The different source apportionment perspectives illustrated in Fig. 3 mainly result from the combined vs. separate approaches for NOx and VOC source apportionment adopted in CMAQ and UCD/CIT, respectively.

3.3. *Ozone source apportionment*

3.3.1. *Model performance analysis*

Fig. 4 illustrates UCD/CIT predictions for O_3 concentrations carried out using spatial resolutions of 24 KM and 4 KM along with observations at four different sites in 2010 September. Simulations carried out at 4 KM spatial resolution predict higher O_3 concentrations during the day and lower O_3 concentrations at night, which generally yields improved performance relative to simulations carried out at 24 KM spatial resolution. Table 3 part (b) shows the model performance statistics for the 4 KM simulations configured with both NOx SA and VOC SA. NMB values are 0.0430 for NOx SA and 0.0372 for VOC SA. NME values are 0.1097 for NOx SA and 0.1086 for VOC SA, and r values are 0.9310 for NOx SA and 0.9307 for VOC SA. Both NMB and NME meet the model performance criteria, and r meets the model performance goals. The statistics indicate that O_3 concentrations predicted by the UCD/CIT model are reasonably accurate.

Figs. S12 and S13 show the UCD/CIT predictions for O_3 concentrations in 2005 July and 2015 August. Table 3 part (c) shows the model performance statistics for the 4 KM simulations in 2005 July. The NMB values for both NOx SA and VOC SA meet the performance criteria. The NME, and r values for both SA meet the performance goal. Table 3 part (d) shows the model performance statistics for the 4 KM simulation in 2015 August. The NMB and r values for both NOx SA and VOC SA slightly exceed the performance criteria. The NME values for both SA meet the performance criteria. Overall, both 2005 and 2015 simulations predict O_3 concentrations with acceptable accuracy.

3.3.2. *Source apportionment*

Fig. 5a–k shows NOx source contributions to O_3 concentrations at hour 12 on Sept 27, 2010. Boundary conditions and initial conditions (BCICs) contribute significantly to O_3 concentrations around the edges of the domain but have decreasing significance at interior locations. NOx emitted from on-road gasoline, off-road gasoline, on-road diesel, and off-road diesel mainly contributes to O_3 formation in urban areas, such as San Francisco and Los Angeles. NOx emitted from wood smoke and food cooking only contributes a very small amount to O_3 formation in the Central Valley of California. NOx emitted from fertilized soils makes widespread contributions to O_3 formation, with a maximum contribution of 55.6 ppb in the Central Valley. NOx emitted from aircraft only contribute to O_3 formation near major airports such as San Francisco International Airport (SFO), Los Angeles International Airport (LAX), and San Diego International Airport (SAN). NOx emitted from natural gas combustion contributes a small amount to O_3 formation in highly urbanized areas.

Fig. 6a–k shows VOC source contributions to O_3 concentrations at hour 12 on Sept 27, 2010. O_3 present in BCICs combined with O_3 formed from VOCs contained in BCICs account for a significant fraction of total O_3 concentrations across the entire state of California. Biogenic emissions also contribute significantly to O_3 formation over the whole

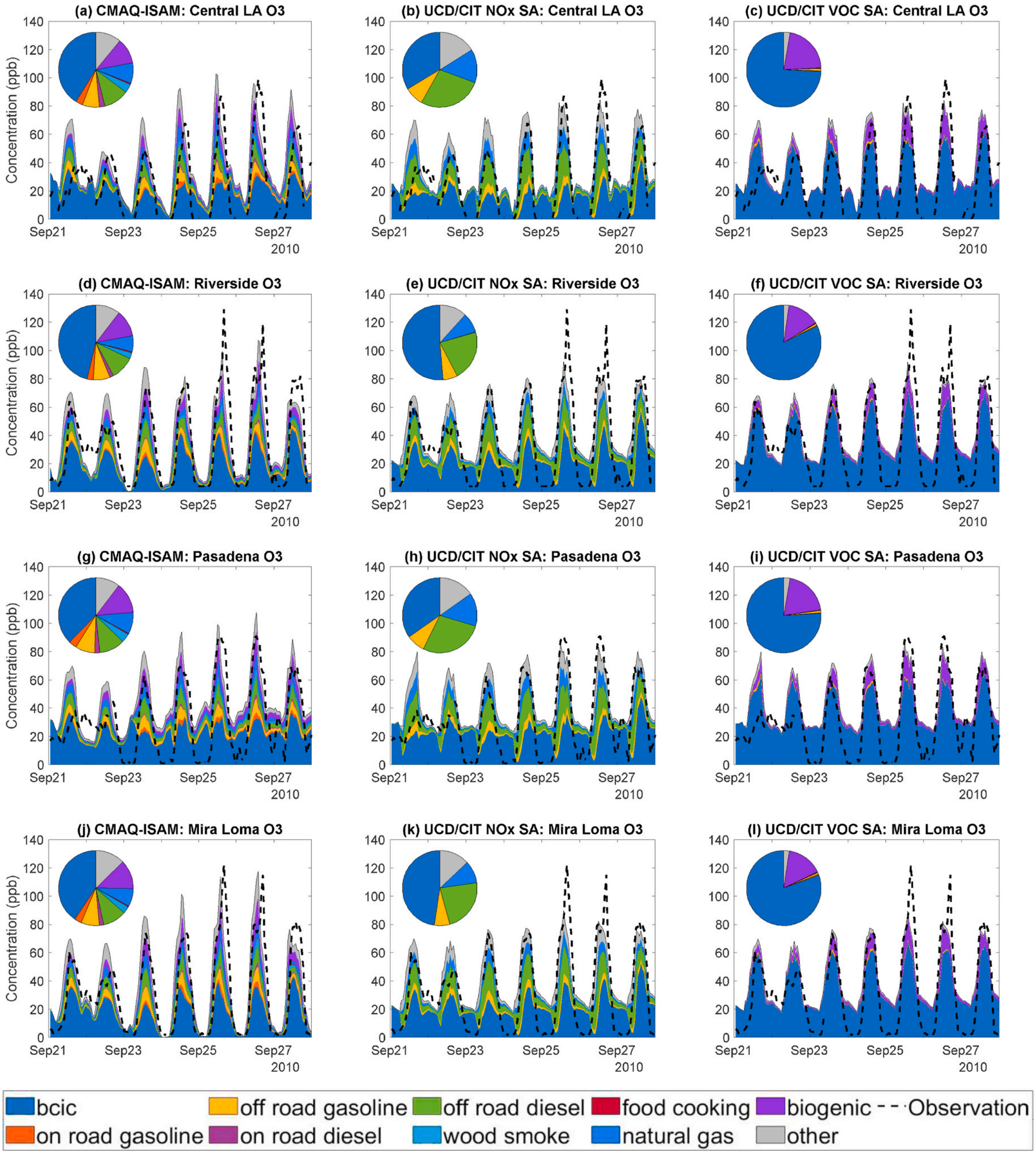

Fig. 3. O_3 source contributions at different sites in 2010 September using the NEI2011 emissions. The left column presents the results of CMAQ-ISAM using O_3 as tagging class. The middle column presents the results of UCD/CIT using NOx SA. The right column presents the results of UCD/CIT using VOC SA. Pie charts are based on O_3 concentrations exceeding 70 ppb.

domain. VOCs emitted from on-road gasoline, off-road gasoline, on-road diesel, off-road diesel, wood smoke and food cooking, aircraft, and natural gas combustion make smaller contributions to O_3 formation. Volatile chemical products (VCPs) included in the ninth source category labelled "other" in Fig. 6 contribute to approximately 4.44 ppb of O_3 formation over Los Angeles with lower contributions in other regions. The implications of potential biases in the VCP inventory (McDonald et al., 2018) are discussed in Section 3.4.2 below.

Figs. 5l and 6l show the O_3 sensitivity regimes for the September 2010 episode using a formaldehyde-to-NO_2 ratio (FNR) (Jin and Holloway, 2015; Liu et al., 2021; Sillman, 1995). A FNR value of 4.6 is used as the transition between the NOx-limited regime and the VOC-limited regime based on the smog chamber experiments conducted by Wu et al., 2022. Figs. 5l and 6l display FNR minus 4.6 so that negative values (blue) indicate VOC-limited conditions and positive values (red) indicate NOx-limited conditions. Most areas of California are VOC-limited during the September 2010 episode.

Figs. S14 and S15 show the NOx and VOC source contributions to O_3 concentrations at hour 12 on Jul. 19, 2005. Figs. S17 and S18 show the NOx and VOC source contributions to O_3 concentrations at hour 12 on Aug. 21, 2015. The spatial pattern of the source contributions in these two years are very similar to the spatial pattern in 2010. The FNR results show that major urban areas and the Central Valley are VOC limited, similar to the patterns observed in Figures 5 and 6 for conditions in 2010.

3.3.3. *Ozone time series plots*

Fig. 7a, c, 7e, 7g show the time-series of NOx source apportionment

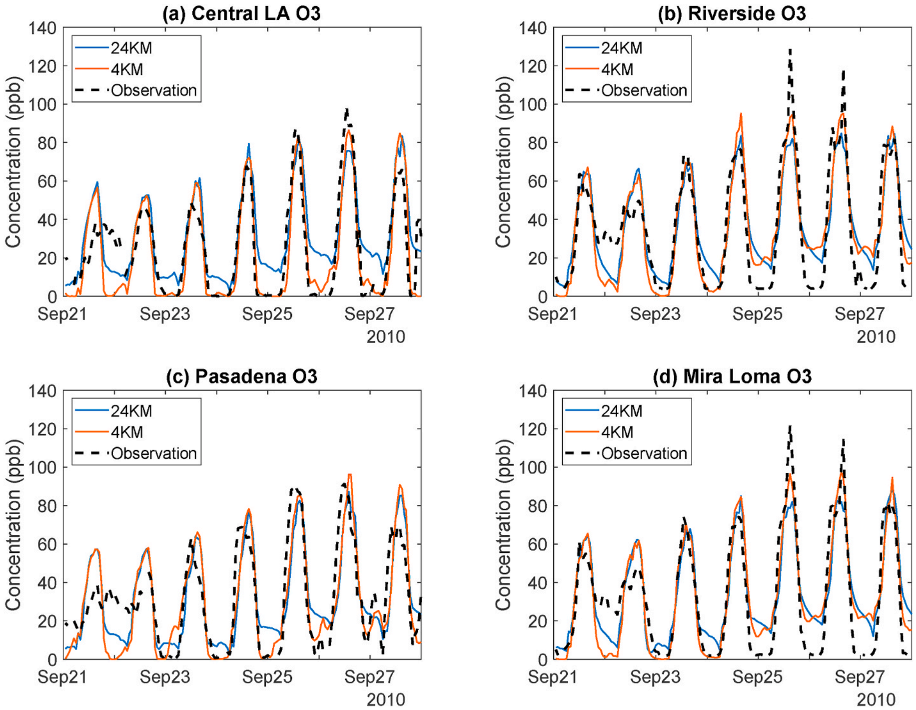

Fig. 4. Time series plot of predicted and measured O_3 concentration in 2010 September at (a) central LA, (b) Riverside, (c) Pasadena, and (d) Mira Loma Van Buren at resolution of 24 KM and 4 KM using NOx SA run results. All simulations use CARB emissions.

results for O_3 concentrations in 2010 September at four different sites in the South Coast Air Basin (SoCAB) surrounding Los Angeles. On-road gasoline, on-road diesel, off-road diesel and soil NOx are the dominant NOx sources contributing to O_3 at all sites. NOx contributions from BCICs are important in Riverside and Mira Loma, but less important in Los Angeles and Pasadena because these sites have higher emissions from anthropogenic sources. NOx emitted from on-road gasoline, off-road diesel and on-road diesel sources account for over 50% of the O_3 formation at the monitoring sites, making NOx from transportation the largest contributor to O_3 formation. Soil NOx was previously identified as a major source of NOx pollution in California (Almaraz et al., 2018). Soil NOx accounts for 7%–13% of the O_3 formation at the monitoring sites in the current study (see Section 4 for an in-depth analysis). NOx contributions from additional sources, including off-road gasoline combustion, natural gas combustion, and aircraft increase peak daytime O_3 concentrations. All of the NOx source contributions to O_3 formation follow a similar time pattern, with minimum contributions at night and maximum contributions at midday.

Fig. 7b, d, 7f, 7h show the VOC source contributions to O_3 concentrations in 2010 September at Los Angeles, Riverside, Pasadena, and Mira Loma. Source apportionment patterns are similar at all four sites. VOCs contained in BCICs make the largest contribution to O_3 formation, followed next by VOC emissions from biogenic sources. VOCs emitted from on-road gasoline and off-road gasoline make smaller contributions (approximated 1% each) to O_3 formation, and remaining sources are even less significant. Implications for potential under-estimates of VCP emissions on these results are discussed in Section 3.4.2 below.

Fig. S16 shows the NOx and VOC source contributions to O_3 concentrations in 2005 July at Los Angeles, Riverside, and Pasadena. The three sites show similar patterns. On-road gasoline, off-road gasoline, and on-road diesel are the three largest NOx source contributors. BCICs and biogenic emissions are the main VOC source contributors. In 2015 August (Fig. S19), the major NOx source contributors are on-road gasoline, on-road diesel, off-road diesel, and soil NOx, while the major VOC source contributors are still BCICs and biogenic emissions.

Fig. 8 illustrates the trend in NOx and VOC source contributions to O_3 formation at Riverside in different time periods. NOx emitted from on-road gasoline and on-road diesel engines make significant contributions to O_3 formation across all time periods. The contribution from off-road gasoline is significant in 2005, but not significant in 2010 and 2015, reflecting the large reduction in emissions from this category (Table S5). Relative contributions from off-road diesel and soil NOx become more important over time as these emissions stay relatively constant while emissions from other sources are reduced. Upwind sources (BCICs) and biogenic emissions are consistently the two major VOC contributors to O_3 formation across all time periods. Off-road gasoline contributes ~6% to O_3 formation in 2005, but has much smaller contributions in later years due to emissions reductions in this category. All the other anthropogenic VOC sources make smaller contributions to O_3 formation in the current simulations. Implications for possible biases in VOC emissions estimates are discussed in Section 3.4.2. Similar trends for O_3 source contributions at other sites in the study domain are shown in Fig. S20.

3.4. Uncertainty analysis

3.4.1. Impact of minor formation channels

The VOC source apportionment results shown in Figs. 6 and 7 indicate that upwind boundary conditions contribute strongly to O_3 formation. This may reflect upwind VOCs or it may reflect upwind O_3 and NO_2 that formed due to the influence of those upwind VOCs. CO has also been identified as an important precursor for O3 formation under relatively low-concentration conditions (Pusede et al., 2014). This formation channel was assumed to be minor in the current study. CO was not tagged and the O_3 formed through the CO reaction channel was assigned to the untagged (i.e. ICBC) source. In order to confirm that this approximate treatment of the CO reaction pathway does not bias the source apportionment results, a separate set of calculations was performed that applied source tags to CO and all of the reaction products involved in this pathway. The predicted spatial distribution of O_3 concentrations associated with individual source types (Fig. S9) is virtually unchanged compared to the results generated without source tagging in

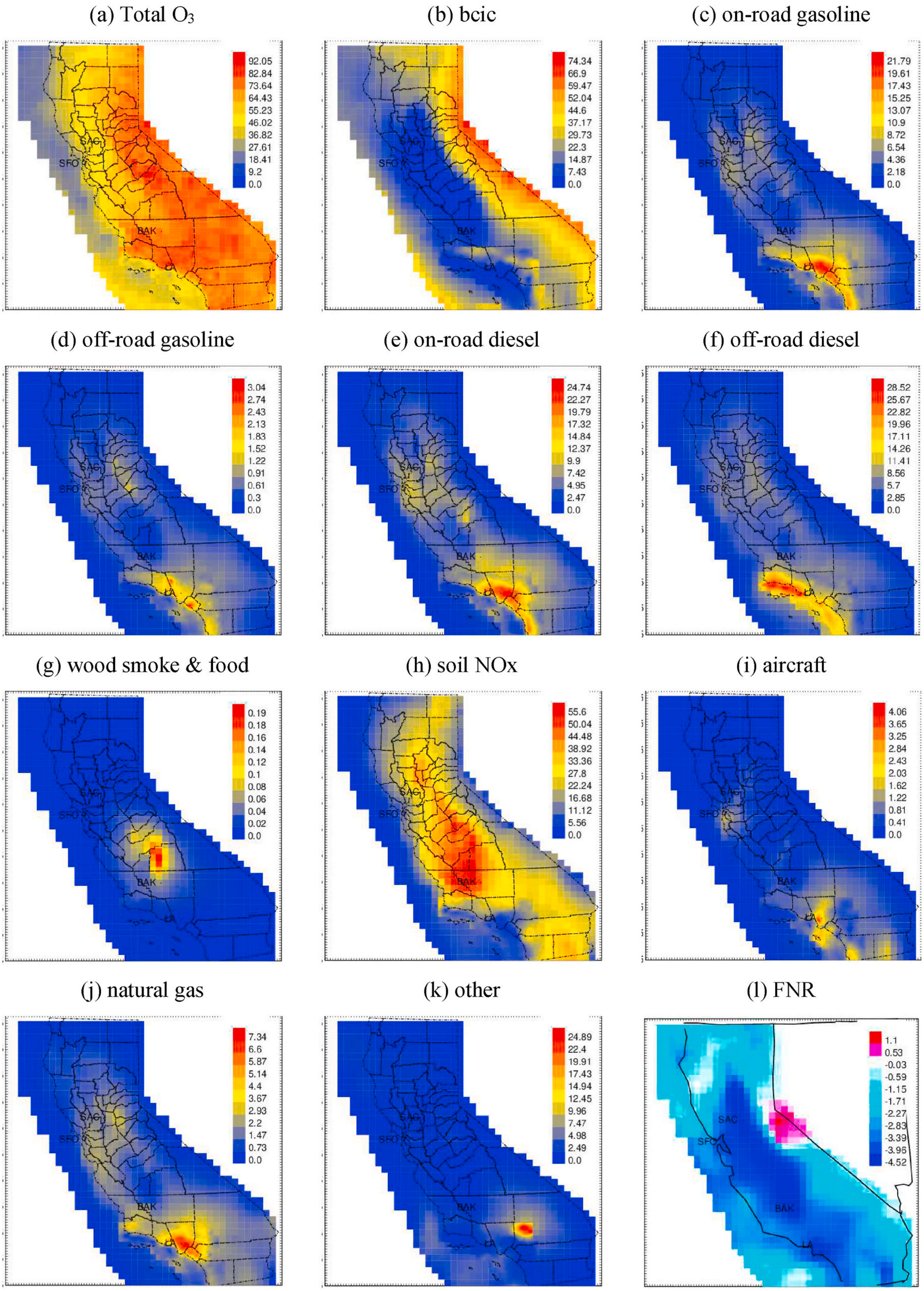

(a) Total O_3

(b) bcic

(c) on-road gasoline

(d) off-road gasoline

(e) on-road diesel

(f) off-road diesel

(g) wood smoke & food

(h) soil NOx

(i) aircraft

(j) natural gas

(k) other

(l) FNR

Fig. 5. (A–k) Predicted NOx source contributions to O_3 concentrations (ppb) and (l) FNR minus 4.6 at h 12, Sep 27, 2010. All simulations use CARB emissions. Note that each plot has different maximum values.

(a) Total O_3 (b) bcic (c) on-road gasoline

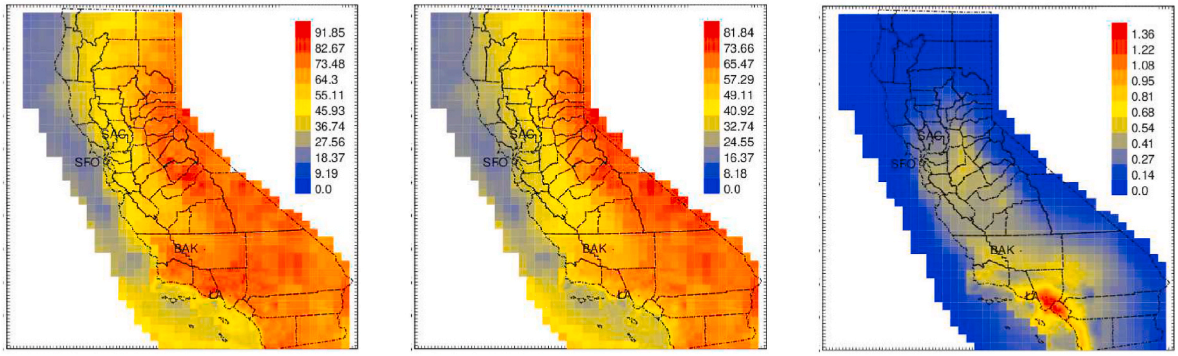

(d) off-road gasoline (e) on-road diesel (f) off-road diesel

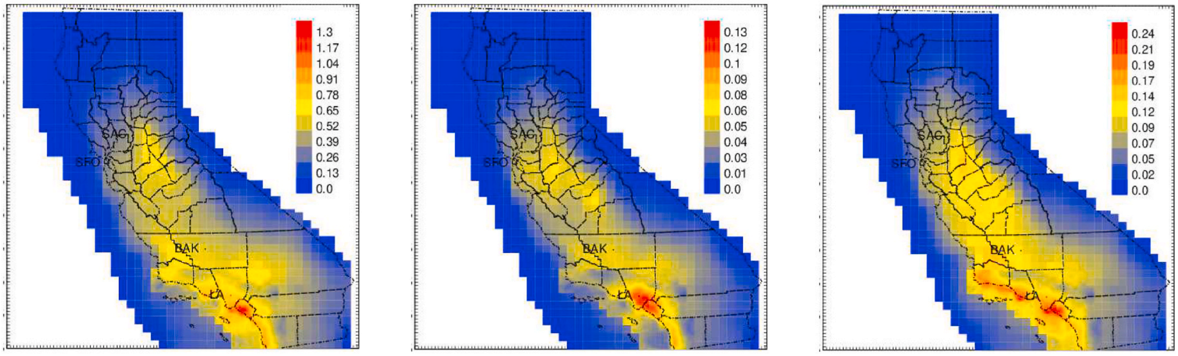

(g) wood smoke & food (h) biogenic (i) aircraft

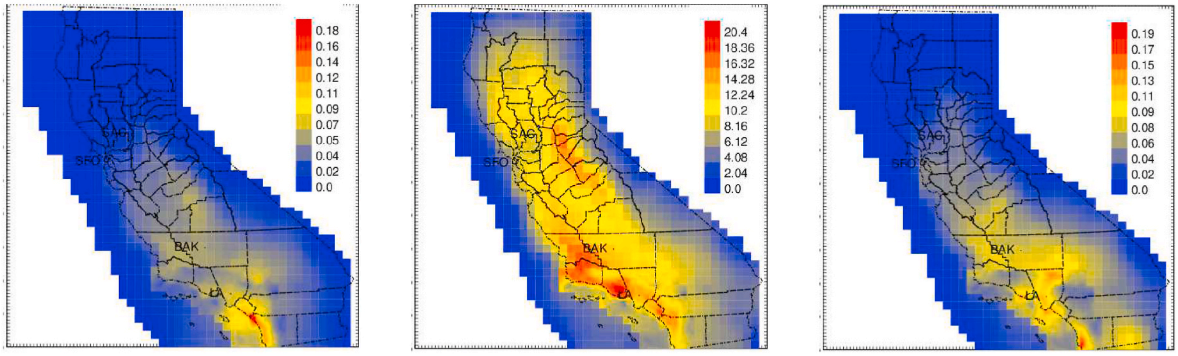

(j) natural gas (k) other (l) FNR

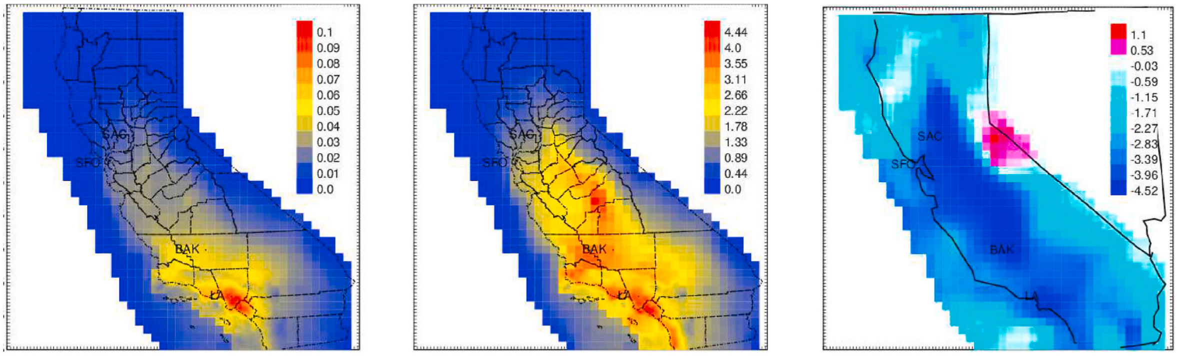

Fig. 6. Predicted VOC source contributions to O_3 concentrations (ppb) at hour 12, Sep 27, 2010. All simulations use CARB emissions. Note that each plot has different maximum values.

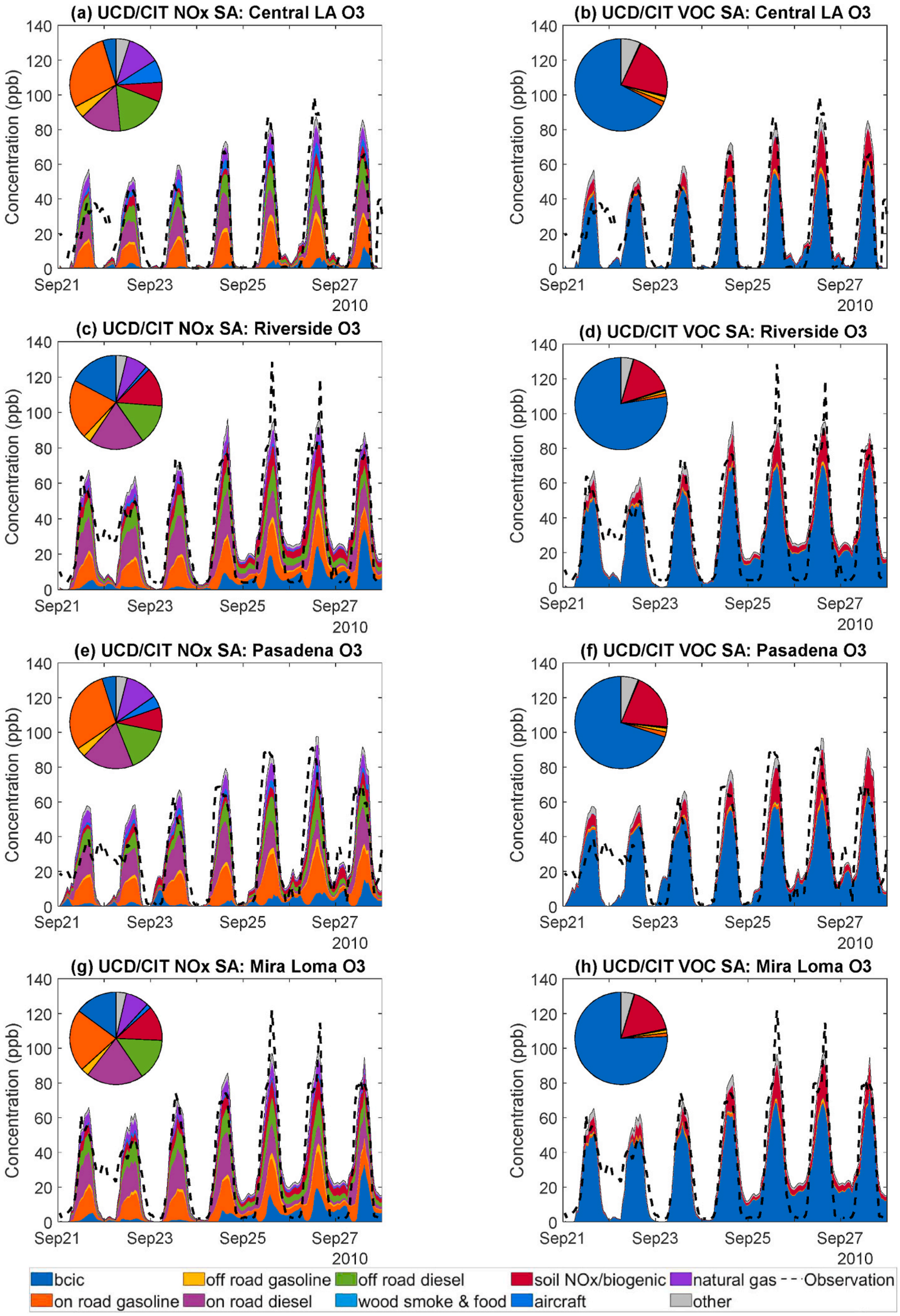

Fig. 7. O_3 source contributions in 2010 September at central LA (a, b), Riverside (c, d), Pasadena (e, f), and Mira Loma Van Buren (g, h) at resolution of 4 KM. Pie charts are based on O_3 concentrations exceeding 70 ppb. All simulations use CARB emissions.

the CO formation channel (Fig. 6). This finding did not change when the CO emission inventory was increased by a factor of five, suggesting that the CO formation pathway does not contribute strongly to O_3 concentrations in Los Angeles. Fig. 9 shows the original O_3 concentrations (Fig. 9a) and the O_3 concentrations when the CO emissions were increased by a factor of five (Fig. 9b). The increased CO emissions only caused a maximum O_3 concentration increase of 3.04 ppb, once again confirming that this formation channel is relatively minor.

3.4.2. *Perturbation analysis for VCP emissions*

McDonald et al. (2018) measured high concentrations of volatile chemical products (VCPs) in the Los Angeles atmosphere and suggested that emissions inventories for VCPs may be under-estimated by a factor of approximately three. A perturbation analysis was carried out in the current study by tripling the VCP emissions (3xVCP) in “other” sources that contain VCPs to examine how this potential bias would influence the O_3 source apportionment results. Fig. 10a shows the change in O_3 concentrations associated with source category 9 “other sources” that included contributions from VCPs caused by the adoption of the 3xVCP emissions. Fig. 10b shows the change in untagged O_3 concentrations associated with boundary conditions caused by the adoption of the 3xVCP emissions. All other source contributions were approximately unchanged. Increasing VCP emissions by a factor of three increased the O_3 concentrations directly produced by VCP emissions by approximately 1.73 ppb. The increased reactivity of the atmosphere also had the indirect effects of increasing O_3 concentrations associated with BCICs by 0.35 ppb over south-east Los Angeles and decreasing O_3 concentrations associated with BCICs by approximately 0.2–0.3 ppb at other locations.

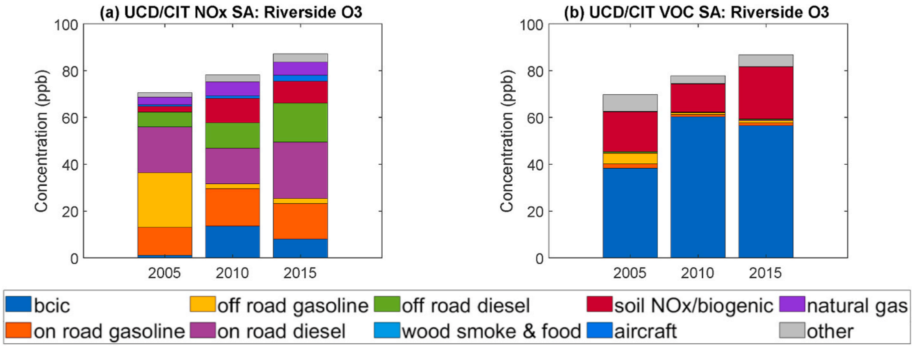

Fig. 8. Trend of O_3 source contributions for (a)NOx SA and (b)VOC SA at Riverside in different episodes when O_3 concentrations exceed 70 ppb.

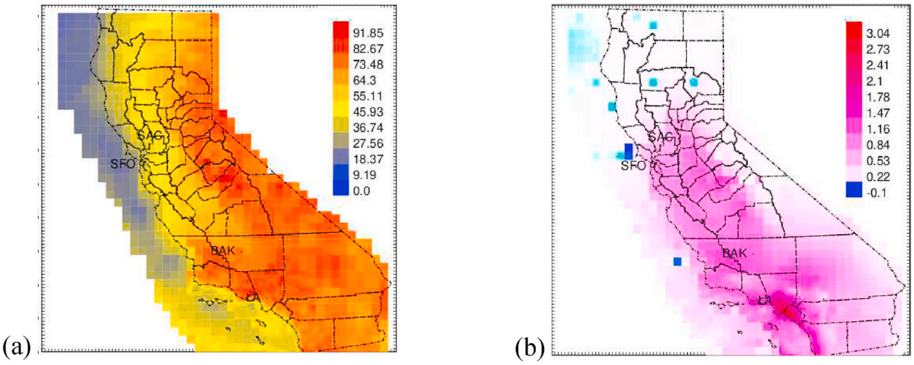

Fig. 9. (A) field plot of original O_3 concentrations at hour 12 of sep27 2010. (b) Increased O_3 concentrations when the CO emissions were increased by a factor of five. All simulations use CARB emissions.

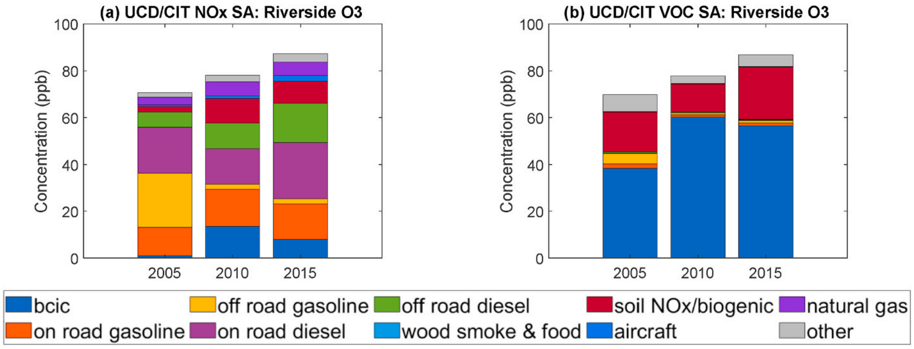

Fig. 10. Field plots of O_3 VOC source contribution differences between 3xVCP and 1xVCP by averaging hour 15 results from 10sep24 to 10sep27. All simulations use CARB emissions.

All these changes are relatively minor compared to the dominance of VOC contributions to O_3 formation from biogenic sources and BCICs illustrated in Fig. 6.

3.4.3. Impact of modified tagging mechanism

It should be noted that the source apportionment results discussed in the previous sections depend on the rules enforced in the tagging mechanism, which may be open to interpretation depending on the desired information. For example, a perturbation analysis was conducted by modifying the following tagged reaction template in NOx SA:

O3[_N1] + NO[_N2] = NO2[_N2] + O2

to

O3[_N1] + NO[_N2] = #.5 NO2[_N1] + #.5 NO2[_N2] + O2

in order to better preserve information describing the impacts of upwind sources contributing to the local O_3 in the presence of the primary photolytic cycle. Fig. 11 shows the modified NOx SA result (right) compared to the original NOx SA result (left) in Los Angeles. O_3 contribution from BCICs are greater than 75% in the modified NOx SA result, dominating over all the other sources even though NOx concentrations in the upwind atmosphere are relatively minor. The modified NOx tagging mechanism effectively weights the identity of the NOx source that contributed to O_3 formation towards the initial NOx source instead of the most recent NOx source. The choice of which approach provides more useful NOx source apportionment information will depend on the preferences of the researcher conducting the analysis. Similar conclusions are reached for source contributions at other sites using the modified NOx tagging mechanism (see Fig. S11).

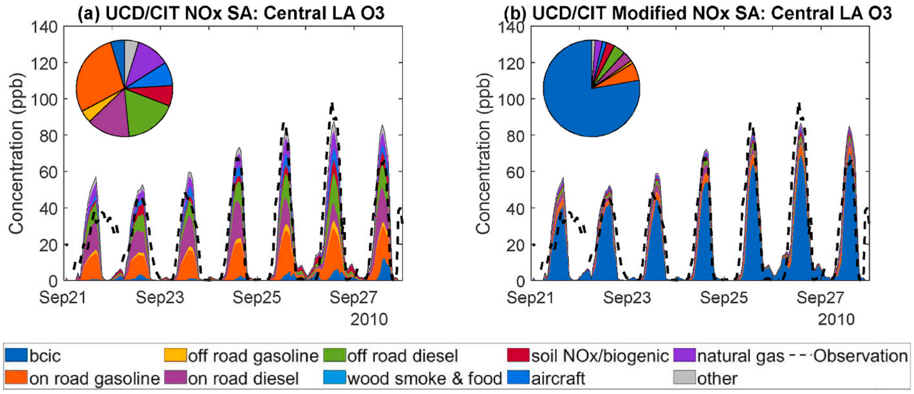

Fig. 11. O_3 NOx source contributions at central LA (a,b) at resolution of 4 KM. Pie charts are based on O_3 concentrations exceeding 70 ppb. All simulations use CARB emissions.

4. Discussion and implications

The lack of anthropogenic VOC sources that contribute to O_3 formation in the current study may reflect biases in the base emissions inventory, but tripling the VCP emissions in the CARB2010 inventory over Los Angeles to account for potential biases had limited impact on O_3 formation during the time period Sept 21–27, 2010. These results are consistent with simulations conducted by Zhu et al. (2019), who found that base-case CMAQ O_3 predictions during the CalNex study period in July 2010 were in good agreement with measurements, and increasing VCP emissions threefold had limited impact on predicted O_3 concentrations (approximately +3 ppb averaged over the SoCAB). Predicted O_3 concentrations did increase (+15 ppb for peak maximum 8-hr O_3 concentrations) when all anthropogenic VOC emissions were scaled upwards, but the resulting concentrations were significantly higher than measured O_3 concentrations, emphasizing the unrealistic nature of this scenario.

The O_3 source apportionment results predicted by the UCD/CIT model and the CMAQ-ISAM model are in good agreement, but the insight gained from the UCD/CIT calculations about the lack of controllable VOC sources within the study domain is helpful when designing practical emissions control programs. The FNR plots show that the Los Angeles area is VOC-limited during each of the three O_3 episodes considered in the present study. Conventional approaches dictate that reducing VOC emissions will provide the most efficient path to control O_3, but the detailed results from the current analysis show that most of the VOCs contributing to O_3 formation over Los Angeles across all time periods originated from upwind boundary conditions outside of the study domain or biogenic emissions within the study domain. Anthropogenic VOC emissions contributed very little to O_3 formation, indicating that reducing anthropogenic VOC emissions might not be an effective O_3 control strategy. In contrast, most of the NOx that contributed to O_3 formation was emitted from anthropogenic sources. Controlling NOx emissions may therefore be the only practical strategy to control O_3 concentrations in the region even though the O_3 formation is VOC limited. Chamber experiments conducted by Wu et al., 2022 in Sacramento between April 2020 and December 2020 also found significant biogenic contributions to O_3 formation in the summer. These measurements also suggest that the most practical strategy to control extreme O_3 concentrations over most of California is to reduce NOx emissions until the atmospheric chemical regime becomes NOx-limited.

It should be noted that the NOx source contributions to O_3 concentrations in the VOC-limited regime are not a literal prediction of the amount of O_3 reduction that would be expected per unit of NOx reduction. The non-linear nature of the photochemical reaction system may even cause O_3 concentrations to increase when NOx emissions from a prevalent source are slightly reduced when conditions are VOC-limited. Two brute force tests were conducted by zeroing out either soil NOx or biogenic emissions. The effects of the brute force are compared with the source contribution from soil NOx in NOx SA and biogenic emissions in VOC SA, respectively (Fig. 12 and Fig. S21). Fig. 12 shows that in Central LA, and Riverside, when soil NOx emissions are zeroed out, O_3 concentrations can either decrease or increase depending on the final chemical regime. In contrast, O_3 concentration reductions due to zeroing out the biogenic emissions are proportional to the VOC source contributions by biogenic emissions. Plots for Pasadena and Mira Loma Van Buren are shown as Fig. S21. For the best interpretation of the SA results, both NOx and VOC SA results should be reviewed together with the chemical regime for further control strategy analysis. Overall, the NOx source apportionment results provide useful information about which NOx sources should be targeted in order to achieve major emissions reductions that would shift the chemical regime to NOx-limited conditions. Once the chemistry has become NOx-limited, the NOx source contributions to O_3 concentrations will be more proportional to the expected O_3 response to NOx emissions reductions.

5. Conclusion

A new O_3 source apportionment method has been developed to separately resolve NOx source contributions and VOC source contributions to O_3 formation within the framework of a chemical transport model (CTM). The new method explicitly tags all molecules that carry odd oxygen within the chemical mechanism rather than making simplifying approximations that follow only a subset of tagged species. Explicitly tracking source-oriented species through the advection calculation required the development of a new Forester filter algorithm to reduce the computational noise induced by sharp wave fronts associated with individual sources. A new algorithm was also developed to efficiently represent reactions involving molecules that contain more than one source of odd oxygen within the source apportionment calculations.

The new source apportionment method was demonstrated using the SAPRC11 chemical mechanism within the UCD/CIT CTM applied to the peak O_3 episodes that occurred in Los Angeles during the years 2005, 2010, and 2015. Total O_3 concentrations and combined NOx + VOC source contributions predicted by the new technique were consistent with results predicted by the CMAQ-ISAM results, but new insights were provided by separately resolving NOx source contributions and VOC source contributions. The three case studies in 2005, 2010, and 2015 over Los Angeles suggest that most of the VOC emissions that contributed to O_3 formation were not controllable, indicating that NOx emissions controls provided the best approach to reducing O_3 concentrations as recently as the year 2015 even though Los Angeles was in the VOC-limited O_3 formation regime. Gasoline-powered vehicles, diesel-powered engines, soil NOx and natural gas combustion are identified as major sources that emit NOx that contribute to O_3 formation. Missing

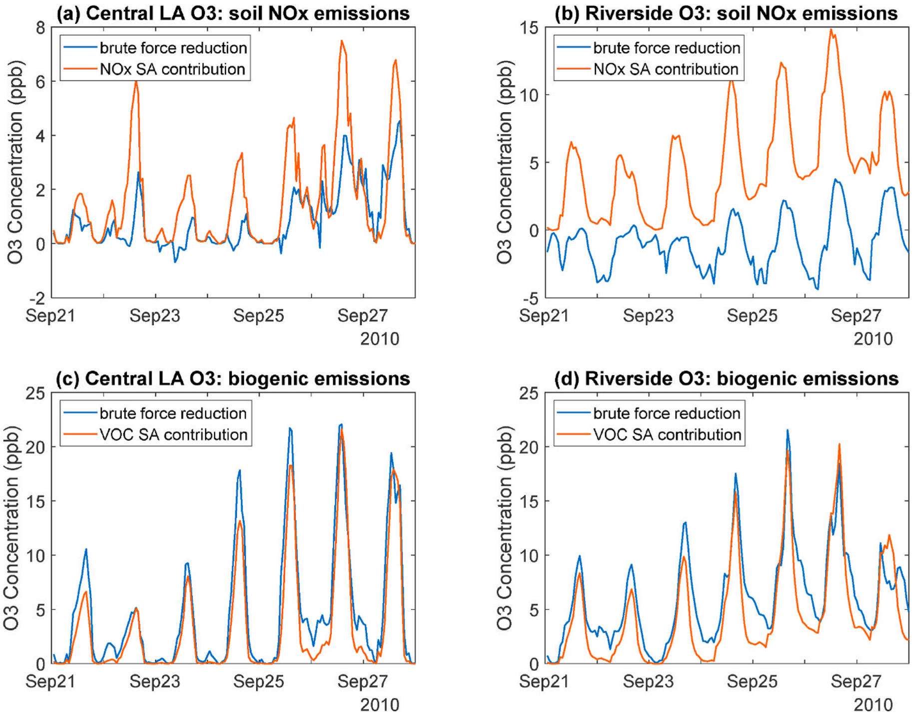

Fig. 12. Comparison of (a, b) the O_3 reductions due to zeroing out soil NOx and the O_3 contribution from soil NOx in the NOx SA results; (c,d) the O_3 reductions due to zeroing out biogenic emissions and the O_3 contribution from biogenic in the VOC SA results. Spatial resolution for all simulations is 4 km.

sources of Volatile Chemical Species (VCPs) may influence the results of this case study, but the overall results of the new source apportionment algorithm are shown to be accurate subject to the uncertainties in the emissions inventory used to support the calculations. This new O_3 source apportionment technique should be useful for current and future simulations that seek to design effective emissions control programs.

CRediT authorship contribution statement

Yusheng Zhao: developed SA mechanisms, performed model simulations, wrote the first draft of manuscript. **Yiting Li:** prepared emissions inventories used for simulations. **Anikender Kumar:** created meteorological fields used for simulations. **Qi Ying:** formulated the simplified SA algorithm. **Francois Vandenberghe:** created meteorological fields used for simulations. **Michael J. Kleeman:** designed the study, debugged SA mechanisms, and helped revise the manuscript.

Declaration of competing interest

The authors declare that they have no known competing financial interests or personal relationships that could have appeared to influence the work reported in this paper.

Acknowledgements

This study was funded by the California Air Resources Board under Contract No. 15AQP010 and the United States Environmental Protection Agency under Grant No. R83587901. The statements and conclusions in this report are those of the contractor and not necessarily those of the California Air Resources Board. The mention of commercial products, their source, or their use in connection with material reported herein is not to be construed as actual or implied endorsement of such products. Although the research described in the article has been funded by the United States Environmental Protection Agency it has not been subject to the Agency's required peer and policy review and therefore does not necessarily reflect the reviews of the Agency and no official endorsement should be inferred.

Appendix A. Supplementary data

Supplementary data to this article can be found online at https://doi.org/10.1016/j.atmosenv.2022.119224.

References

Almaraz, M., Bai, E., Wang, C., Trousdell, J., Conley, S., Faloona, I., Houlton, B.Z., 2018. Agriculture is a major source of NOx pollution in California. Sci. Adv. 4 (6), 1–9. https://doi.org/10.1126/SCIADV.AAU2561.

Atkinson, R., 2000. Atmospheric chemistry of VOCs and NOx. Atmos. Environ. 34 (12–14), 2063–2101. https://doi.org/10.1016/S1352-2310(99)00460-4.

Burnett, R.T., Brook, J.R., Yung, W.T., Dales, R.E., Krewski, D., 1997. Association between ozone and hospitalization for respiratory diseases in 16 Canadian cities. Environ. Res. 72 (1), 24–31. https://doi.org/10.1006/enrs.1996.3685.

Carter, W.P.L., Heo, G., 2013. Development of revised SAPRC aromatics mechanisms. Atmos. Environ. 77, 404–414. https://doi.org/10.1016/j.atmosenv.2013.05.021.

Chock, D.P., 1985. A comparison of numerical methods for solving the advection equation-II. Atmos. Environ. 19 (4), 571–586.

Chock, D.P., 1991. A comparison of numerical methods for solving the advection equation-III. Atmos. Environ. 25 (5), 853–871.

Chock, D.P., Dunker, A.M., 1983. A comparison of numerical methods for solving the advection equation. Atmos. Environ. 17 (1), 11–24.

Cohan, D.S., Napelenok, S.L., 2011. Air quality response modeling for decision support. Atmosphere 2 (3), 407–425. https://doi.org/10.3390/atmos2030407.

Collet, S., Kidokoro, T., Karamchandani, P., Jung, J., Shah, T., 2018. Future year ozone source attribution modeling study using CMAQ-ISAM. J. Air Waste Manag. Assoc. 68 (11), 1239–1247. https://doi.org/10.1080/10962247.2018.1496954.

Collet, S., Minoura, H., Kidokoro, T., Sonoda, Y., Kinugasa, Y., Karamchandani, P., Johnson, J., Shah, T., Jung, J., Denbleyker, A., 2014. Future year ozone source attribution modeling studies for the eastern and western United States. J. Air Waste Manag. Assoc. 64 (10), 1174–1185. https://doi.org/10.1080/10962247.2014.936629.

Dunker, A.M., Yarwood, G., Ortmann, J.P., Wilson, G.M., 2002. Comparison of source apportionment and source sensitivity of ozone in a three-dimensional air quality model. Environ. Sci. Technol. 36 (13), 2953–2964. https://doi.org/10.1021/es011418f.

Emery, C., Liu, Z., Russell, A.G., Odman, M.T., Yarwood, G., Kumar, N., 2017. Recommendations on statistics and benchmarks to assess photochemical model performance. J. Air Waste Manag. Assoc. 67 (5), 582–598. https://doi.org/10.1080/10962247.2016.1265027.

Faloona, I.C., Chiao, S., Eiserloh, A.J., Alvarez, R.J., Kirgis, G., Langford, A.O., Senff, C.J., Caputi, D., Hu, A., Iraci, L.T., Yates, E.L., Marrero, J.E., Ryoo, J.M., Conley, S., Tanrikulu, S., Xu, J., Kuwayama, T., 2020. The California baseline ozone transport study (CABOTS). Bull. Am. Meteorol. Soc. 101 (4), E427–E445. https://doi.org/10.1175/BAMS-D-18-0302.1.

Forester, C.K., 1977. Higher order monotonic convective difference schemes. J. Comput. Phys. 23 (1), 1–22. https://doi.org/10.1016/0021-9991(77)90084-5.

Gao, J., Zhu, B., Xiao, H., Kang, H., Hou, X., Shao, P., 2016. A case study of surface ozone source apportionment during a high concentration episode, under frequent shifting wind conditions over the Yangtze River Delta, China. Sci. Total Environ. 544, 853–863. https://doi.org/10.1016/j.scitotenv.2015.12.039.

Gao, J., Zhu, B., Xiao, H., Kang, H., Hou, X., Yin, Y., Zhang, L., Miao, Q., 2017. Diurnal variations and source apportionment of ozone at the summit of Mount Huang, a rural site in Eastern China. Environ. Pollut. 222, 513–522. https://doi.org/10.1016/j.envpol.2016.11.031.

Gent, J.F., Triche, E.W., Holford, T.R., Belanger, K., Bracken, M.B., Beckett, W.S., Leaderer, B.P., 2003. Association of low-level ozone and fine particles with respiratory symptoms in children with asthma. JAMA 290 (14), 1859–1867.

Jin, X., Holloway, T., 2015. Spatial and temporal variability of ozone sensitivity over China observed from the Ozone Monitoring Instrument. J. Geophys. Res. Atmos. 120, 7229–7246. https://doi.org/10.1038/175238c0.

Kleeman, M.J., Cass, G.R., 2001. A 3D Eulerian source-oriented model for an externally mixed aerosol. Environ. Sci. Technol. 35 (24), 4834–4848. https://doi.org/10.1021/es010886m.

Kleeman, M.J., Ying, Q., Kaduwela, A., 2005. Control strategies for the reduction of airborne particulate nitrate in California's San Joaquin Valley. Atmos. Environ. 39 (29), 5325–5341. https://doi.org/10.1016/j.atmosenv.2005.05.044.

Kwok, R.H.F., Baker, K.R., Napelenok, S.L., Tonnesen, G.S., 2015. Photochemical grid model implementation and application of VOC, NOx, and O3 source apportionment. Geosci. Model Dev. (GMD) 8 (1), 99–114. https://doi.org/10.5194/gmd-8-99-2015.

Lee, D.S., Holland, M.R., Falla, N., 1996. The potential impact of ozone on materials in the U.K. Atmos. Environ. 30 (7), 1053–1065. https://doi.org/10.1016/1352-2310(95)00407-6.

Li, Y., Lau, A.K.H., Fung, J.C.H., Zheng, J.Y., Zhong, L.J., Louie, P.K.K., 2012. Ozone source apportionment (OSAT) to differentiate local regional and super-regional source contributions in the Pearl River Delta region, China. J. Geophys. Res. Atmos. 117 (15), 1–18. https://doi.org/10.1029/2011JD017340.

Lippmann, M., 1989. Effects of ozone on respiratory function and structure. Annu. Rev. Publ. Health 10 (26), 49–67. https://doi.org/10.1146/annurev.publhealth.10.1.49.

Liu, J., Li, X., Tan, Z., Wang, W., Yang, Y., Zhu, Y., Yang, S., Song, M., Chen, S., Wang, H., Lu, K., Zeng, L., Zhang, Y., 2021. Assessing the ratios of formaldehyde and glyoxal to NO 2 as indicators of O 3 −NO x −VOC sensitivity. Cite This: Environ. Sci. Technol. 55, 10935–10945. https://doi.org/10.1021/acs.est.0c07506.

McDonald, B.C., De Gouw, J.A., Gilman, J.B., Jathar, S.H., Akherati, A., Cappa, C.D., Jimenez, J.L., Lee-Taylor, J., Hayes, P.L., McKeen, S.A., Cui, Y.Y., Kim, S.W., Gentner, D.R., Isaacman-VanWertz, G., Goldstein, A.H., Harley, R.A., Frost, G.J., Roberts, J.M., Ryerson, T.B., Trainer, M., 2018. Volatile chemical products emerging as largest petrochemical source of urban organic emissions. Science 359 (6377), 760–764. https://doi.org/10.1126/science.aaq0524.

Pusede, S.E., Gentner, D.R., Wooldridge, P.J., Browne, E.C., Rollins, A.W., Min, K.E., Russell, A.R., Thomas, J., Zhang, L., Brune, W.H., Henry, S.B., Digangi, J.P., Keutsch, F.N., Harrold, S.A., Thornton, J.A., Beaver, M.R., Clair, St, J, M., Wennberg, P.O., Sanders, J., et al., 2014. On the temperature dependence of organic reactivity, nitrogen oxides, ozone production, and the impact of emission controls in San Joaquin Valley, California. Atmos. Chem. Phys. 14 (7), 3373–3395. https://doi.org/10.5194/acp-14-3373-2014.

Rich, S., 1964. Ozone damage to plants. Annu. Rev. Phytopathol. 2 (1), 253–266. https://doi.org/10.1146/annurev.py.02.090164.001345.

Sillman, S., 1995. The use of NOy, H2O2, and HNO3 as indicators for ozone-NOx-hydrocarbon sensitivity in urban locations. J. Geophys. Res. 100, 175–188.

Tonnesen, G.S., Dennis, R.L., 2000. Analysis of radical propagation efficiency to assess ozone sensitivity to hydrocarbons and NOx 1. Local indicators of instantaneous odd oxygen production sensitivity. J. Geophys. Res. Atmos. 105 (D7), 9213–9225. https://doi.org/10.1029/1999JD900371.

Venecek, M.A., Yu, X., Kleeman, M.J., 2019. Predicted ultrafine particulate matter source contribution across the continental United States during summertime air pollution events. Atmos. Chem. Phys. 19 (14), 9399–9412. https://doi.org/10.5194/acp-19-9399-2019.

Wu, S., Lee, H.J., Rohrbacher, A., Liu, S., Kuwayama, T., Seinfeld, H., Kleeman, M.J., 2022. Direct measurements of ozone response to emissions perturbations in California. Atmos. Chem. Phys. 22 (7), 4929–4949. https://doi.org/10.5194/acp-2021-708/.

Ying, Q., Kleeman, M.J., 2006. Source contributions to the regional distribution of secondary particulate matter in California. Atmos. Environ. 40 (4), 736–752. https://doi.org/10.1016/j.atmosenv.2005.10.007.

Ying, Q., Mysliwiec, M.J., Kleeman, M.J., 2004. Source apportionment of visibility impairment using a three-dimensional source-oriented air quality model. Environ. Sci. Technol. 38 (4), 1089–1101. https://doi.org/10.1021/es0349305.

Yu, X., Venecek, M., Kumar, A., Hu, J., Tanrikulu, S., Soon, S.T., Tran, C., Fairley, D., Kleeman, M.J., 2019. Regional sources of airborne ultrafine particle number and mass concentrations in California. Atmos. Chem. Phys. 19 (23), 14677–14702. https://doi.org/10.5194/acp-19-14677-2019.

Zhu, S., Kinnon, M. Mac, Shaffer, B.P., Samuelsen, G.S., Brouwer, J., Dabdub, D., 2019. An uncertainty for clean air: air quality modeling implications of underestimating VOC emissions in urban inventories. Atmos. Environ. 211, 256–267. https://doi.org/10.1016/j.atmosenv.2019.05.019.